

Contract No.:

This manuscript has been authored by Savannah River Nuclear Solutions (SRNS), LLC under Contract No. DE-AC09-08SR22470 with the U.S. Department of Energy (DOE) Office of Environmental Management (EM).

Disclaimer:

The United States Government retains and the publisher, by accepting this article for publication, acknowledges that the United States Government retains a non-exclusive, paid-up, irrevocable, worldwide license to publish or reproduce the published form of this work, or allow others to do so, for United States Government purposes.

Ab initio GGA+U investigations of the structural, electronic and magnetic properties of $\text{Cd}_{1-x}\text{Mn}_x\text{Te}$ alloy

I. M. Yuriychuk^a, P. M. Fochuk^a, A. E. Bolotnikov^b, and R. B. James^c
^aYuriy Fedkovych Chernivtsi National University, 58012 Chernivtsi, Ukraine;
^bBrookhaven National Laboratory, Upton, NY, USA; ^cSavannah River National Laboratory, Aiken, SC, USA

ABSTRACT

The structural, electronic and magnetic properties of $\text{Cd}_{1-x}\text{Mn}_x\text{Te}$ alloy in the zinc-blende (ZB) phase were studied within the framework of spin-polarized density functional theory using the generalized gradient approximation (GGA). We employed the GGA+ U^{SIC} (GGA method plus self-interaction correction potential), which gives a better description of systems with strong Coulomb correlations of the d -electrons. In this paper, we first discuss implementation of the GGA+U method to the ground state calculations of pure CdTe and ferromagnetic MnTe. The alloys are modelled at selected compositions as ordered structures described in terms of periodically repeated supercells for the compositions of $x = 0.25, 0.5$, and 0.75 . The compositional dependences of the lattice constant, electronic band structure and partial densities of states of the ferromagnetic $\text{Cd}_{1-x}\text{Mn}_x\text{Te}$ alloy were also studied. We estimated the spin-exchange splitting energies produced by the Mn $3d$ -states and determined the exchange constants for the conduction and valence bands of the alloy. The energy positions of the occupied and unoccupied Mn $3d$ -bands in the electronic structure of the ferromagnetic $\text{Cd}_{1-x}\text{Mn}_x\text{Te}$ alloy are also presented. Our calculations based on the GGA+ U^{SIC} approach agree well with the available experimental data and other calculations.

Keywords: $\text{Cd}_{1-x}\text{Mn}_x\text{Te}$ alloy, ferromagnetic MnTe, DFT calculations, GGA+U, band structure, magnetic properties.

1. INTRODUCTION

The simultaneous semiconducting and magnetic behaviors of different materials bring about interesting magnetic, magneto-optic, and magneto-transport effects [1, 2]. One of the promising materials of such types are diluted magnetic semiconductors, which have attracted a great deal of interest over the last decades due to the possibility to produce a ferromagnetic semiconductor at room temperatures [2]. Among diluted magnetic semiconductors, much focus has been paid to $\text{Cd}_{1-x}\text{Mn}_x\text{Te}$, which can form homogeneous alloys for x ranging from 0 to 0.75 [3, 4]. $\text{Cd}_{1-x}\text{Mn}_x\text{Te}$ alloy crystallizes in the zinc-blende (ZB) structure where random Cd cation sites are replaced by transitional metal magnetic Mn^{2+} ions, whose electronic $3d$ -shell is half-filled producing a spin value of $5/2$. The d - d exchange interaction of coupled magnetic ions causes formation of spin-glass and antiferromagnetic phases [3, 5], although ferromagnetic ordering at low temperatures has also been observed [4]. The most prominent feature of diluted magnetic semiconductors is a coexistence of different electronic subsystems: delocalized conduction, valence band electrons and localized electrons of magnetic ions [1]. In particular, a large sp - d exchange interaction between the charge carriers and the magnetic ions leads to strong band splitting in $\text{Cd}_{1-x}\text{Mn}_x\text{Te}$ crystals, which results in the giant Faraday rotation and Zeeman splitting [1, 6]. Recently, $\text{Cd}_{1-x}\text{Mn}_x\text{Te}$ alloy was proposed as a material for nuclear radiation detectors [7, 8] due to its good electron transport properties and high resistivity [9, 10].

In view of its great technological importance, $\text{Cd}_{1-x}\text{Mn}_x\text{Te}$ alloy has been a subject of various theoretical investigations, from empirical [11] to first principles based on the density functional theory (DFT) [12-19]. Although the overall picture regarding its structural, electronic and optical properties has been thoroughly studied, some details concerning energy position and hybridization of the Mn $3d$ -state are still questionable. Most of the published ab initio studies were performed using the pseudo-potential or the full-potential linearized-augmented plane wave methods within the local density approximation (LDA) [12] or the generalized gradient approximation (GGA) [13-19]. One of the main drawbacks of DFT approximations, such as the LDA and GGA, is the underestimation the band gap of semiconductors and insulators compared to the experimental gaps. Many theoretical studies were undertaken to obtain better agreement with experiments, such as LDA/GGA+U correction [20], B3LYP function calculations [21], Hybrid Heyd-Scuseria-

Ernzerh (HSE) functionals [22], GW implementations [23], among others. The computational cost of B3LYP, HSE or GW calculations is increased by one or two orders of magnitude compared to LDA/GGA+U calculations. Furthermore, the on-site Coulomb interaction (Hubbard U) leads to a better description of many systems with strong Coulomb correlations of the $3d$ -electrons. Recently, the so-called GGA+U^{SIC} method [24, 25] was applied to self-consistent calculations of structural and electronic properties of CdTe [26]. It was demonstrated that the accuracy of this method is comparable with that of the hybrid functional HSE method and gives better values for the lattice constant and the bulk modulus, but with less computational cost.

In the present work, we apply the GGA+U^{SIC} method for the calculations of the structural, electronic and magnetic properties of pure CdTe, ferromagnetic MnTe and Cd_{1-x}Mn_xTe alloy. The paper is organized as follows. The computational methods are explained in Section 2. Implementation of the GGA+U^{SIC} method to ground state calculations of pure CdTe and ferromagnetic MnTe is presented in Section 3. The results obtained for the structural, electronic and magnetic properties of Cd_{1-x}Mn_xTe alloy are discussed in Section 4. In Section 5 we summarize the main conclusions of this work.

2. COMPUTATIONAL METHODS

The calculations of the structural, electronic, and magnetic properties of Cd_{1-x}Mn_xTe alloy were performed within a framework of the spin-polarized density functional theory using the plane-wave pseudopotential code ABINIT [27]. The GGA approximation parameterized by Perdew–Burke–Ernzerhof (PBE) [28] was used to describe the exchange and correlation effects. Pseudopotentials and all-electron-like wavefunctions were described based on the projector-augmented wave (PAW) method [29]. The following initial atomic configurations were employed: $3d^{10}4s^2$ (Cd), $5s^25p^4$ (Te), and $3d^54s^2$ (Mn). The electron wavefunctions were expanded in a plane-wave basis with 410-eV cutoff energy. The Brillouin zone integrations were performed using k -point grid set (6x6x6) generated according to the Monkhorst–Pack scheme [30]. The self-consistent convergence of the total energy was set to 1.0^{-6} eV/atom. All input parameters have been tested to ensure well converged results.

We modelled alloys with several selected compositions: $x = 0.25, 0.5, 0.75$ in terms of periodically repeated supercells. The basic cubic cell was chosen as a unit cell. Describing random alloys by periodic structures introduces spurious correlations beyond certain distances. Preventing this problem needs very large supercells for which first-principle calculations are still impractical. In this study, the special quasi-random structure (SQS) approach [31] is applied, which effectively reduces the size of the supercell (to 8–32 atoms per unit cell) for studying the properties of the random alloys. For $x = 0.25$ and 0.75 the simplest structure is an eight-atom cubic cell, in which the anions form a regular simple cubic lattice. For the composition $x = 0.5$, the smallest ordered structure is a four-atom tetragonal cell, corresponding to the (001) superlattice. This structure is strongly anisotropic, and thus not very suitable for simulating random alloys [31]. Therefore, we consider also the chalcopyrite structure, which has a 16-atom tetragonal cell. So, for the Mn concentration $x = 0.25$ and $x = 0.75$, a cubic supercell composed of 8 atoms (4 Te atoms, 3 Cd atoms, 1 Mn atom and 4 Te atoms, 1 Cd atom, 3 Mn atoms, respectively) is considered. In the case of Mn with the concentration $x = 0.5$, we used a supercell that is formed of 16 atoms (8 Te atoms, 4 Cd atoms and 4 Mn atom). For comparisons, all calculations for parent compounds CdTe and MnTe were obtained for an 8 atom cubic supercell. In addition, we perform the structural optimization by calculating the total energies for different volumes around the equilibrium cell volume. The calculated total energies were fitted using the Murnaghan’s equation of state to determine the ground state properties, such as the equilibrium lattice constant and the bulk modulus.

3. GGA+U^{SIC} CALCULATIONS FOR CdTe AND MnTe

3.1 Structural and electronic properties of CdTe

CdTe and MnTe are the basic constituents, corresponding to $x = 0$ and 1 in the Cd_{1-x}Mn_xTe alloy. We begin by discussing the calculations for the pure CdTe, using DFT without and with U corrections. It is well known, that DFT is not suitable for describing excited-state properties, such as the energy gap. The band gap of CdTe, calculated within conventional GGA-PBE method is only 0.57 eV, which is much less than the experimental value of 1.61 eV [32]. The calculations with inclusion of the Cd d - d intra-atomic Coulomb energy U_d within GGA+ U approach slightly improve the band-gap values, but not totally. The band gap increases with increasing U_d value at the beginning, but the band gap almost stays constant when the U_d value for Cd $3d$ -orbitals is larger than 7 eV. The calculated band gap (using $U_d = 6$ eV correction) is 0.97 eV, which is still far from the experimental value.

Applying a self-interaction correction (SIC) potential to the $5p$ -orbitals of Te can fix the problem [24]. Moreover, the solution to the problem is acquired at negative values of U_p due to an overestimation of the exchange-correlation hole by the GGA [25]. The predictions of physical properties of the material by the GGA+U^{SIC} method are similar to or better than those obtained with hybrid functionals [26]. We found that the effect of U_p on the band gap of CdTe is somewhat larger than that of U_d , although it tends to saturate. The experimental band gap of 1.61 eV for CdTe was determined when the Hubbard U values of the Cd $3d$ -orbitals and the Te $5p$ -orbitals were set up for $U_d = 6$ eV and $U_p = -14$ eV, respectively.

The calculated within GGA+U^{SIC} method equilibrium lattice constant a and bulk modulus B of CdTe are presented in Table 1, which also contains the results of previous calculations and experimental data. The lattice constant is 0.17% larger than the experimental value, which is the usual level of accuracy of the GGA. The calculated value of bulk modulus is also close to experimental one especially if compared with those calculated within a conventional PBE-GGA.

Table 1. Calculated band gap E_g (in eV), lattice constant a (in Å), bulk modulus B (in GPa), magnetic moment μ (in Bohr magneton μ_B), conduction ΔE_c and valence ΔE_v (in eV) band-edge spin-splitting and exchange constants $N_0\alpha$, $N_0\beta$ (in eV) for CdTe and ferromagnetic MnTe.

	E_g (eV)	a (Å)	B (GPa)	μ (μ_B)	$\Delta E_c, \Delta E_v$ (eV)	$N_0\alpha, N_0\beta$ (eV)	References
CdTe	1.61	6.533	42.51				Present
	1.52	6.568					HSE [33]
		6.424	44.38				LSDA [15]
		6.604	37.02				PBE-GGA [14]
	0.54	6.499	45.76				WC-GGA [18]
		6.481	44.50				Exp. [32]
MnTe	1,78 (up) 4,10 (down)	6.351	45.34	4.422	-1.91, 0.41	-0.86, 0.19	Present
	1.71 (up) 4.5 (down)			4.50	-1.95, 0.79	-0.87, 0.35	GW [34]
		6.50	36.04	4.617			PBE-GGA-U [35]
		6.392	38.10	4.096	-2.36, 0.71	-1.20, 0.34	PBE-GGA [36]
		6.402		4.24			PW-GGA [37]
		6.338					Exp. [38]
							-0.88, 0.22 Exp. [39]

Fig. 1 (a) shows calculations of the electronic band structure of CdTe within the GGA+U^{SIC} method along selected high-symmetry directions of the Brillouin zone. The zero energy was placed at the valence band maximum (VBM), and the dotted line represents the position of the Fermi energy. The partial density of states (PDOS) for CdTe (Fig. 1(b)) shows that the upper part of the valence band (from -5 to 0 eV) contains the Te $5p$ -states coupled with the Cd $4p$ -states and $4s$ -states. The unoccupied bands in the lowest energies of the conduction band consist of the s - and p -states from the Cd atom and the p -states from the Te atom. Here, the p -states of the Cd atom seem to be dominant.

3.2 Electronic and magnetic properties of MnTe

MnTe usually crystallizes in the hexagonal NiAs structure; however, at low temperatures, the metastable zinc-blende epitaxial MnTe layers with a lattice constant $a=6.338$ Å were also grown on cubic substrates [38]. The calculated within GGA+U^{SIC} method equilibrium lattice constant a and bulk modulus B for ferromagnetic MnTe are listed in Table 1. They are in good agreement with the results of other studies and available experimental data.

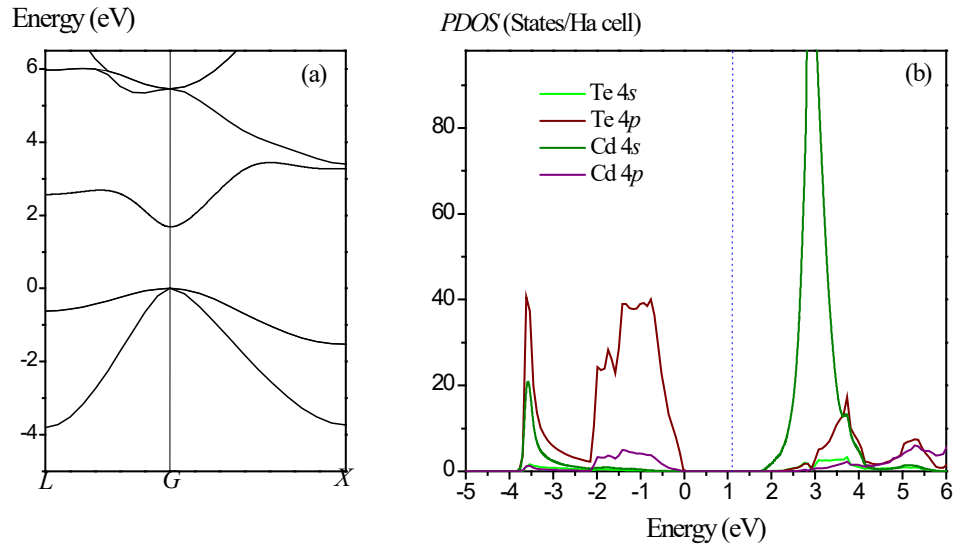


Fig. 1. Electronic band structure (a) and partial density of states (b) for CdTe.

The results of spin-polarized band structure calculations within the GGA+U^{SIC} method for hypothetical ZB ferromagnetic MnTe are presented in Fig. 2. The zero-energy point is placed at the VBM for the spin-up case. The dotted line indicates the position of the Fermi energy. As seen from Fig. 2, the VBM and the conduction band maximum (CBM) are located at the center of the Brillouin zone (G point) confirming the direct gap feature of MnTe. The width of the gap was found to be 1.78 eV and 4.10 eV for the spin-up and spin-down cases, respectively. These values agree well with GW calculations (Table 1). We take the same Hubbard value $U_p = -14$ eV for Te 5*p*-orbitals as for CdTe. Our Hubbard correction for the Mn 3*d*-orbitals $U_d = 4.5$ eV is in accordance with the known values in the literature of $U_d \approx 4$ eV, which give a sufficient description of the ground-state properties of ZB ferromagnetic MnTe [35].

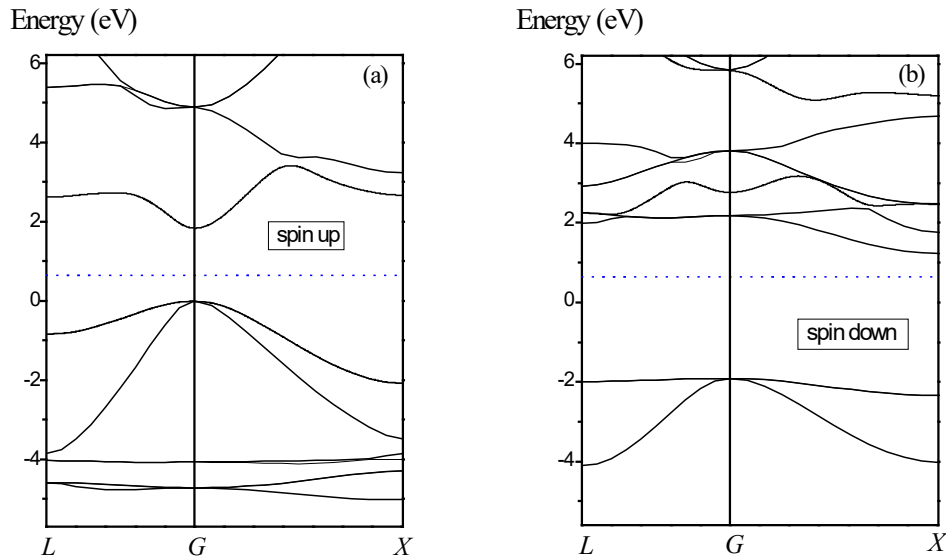


Fig. 2. Electronic band structure of ferromagnetic MnTe for spin-up (a) and spin-down (b) cases. The dotted line indicates the position of the Fermi energy.

The spin-dependent partial density of states for the Mn and Te sites are presented in Fig. 3. For the spin-up case, the Mn 3*d*-states are mixed with the Te 5*p*-states, whereas for the spin-down case the Mn 3*d*-states are unoccupied. Note that the lowest conduction bands are formed predominantly from the Te 5*s*- and 5*p*-orbitals for the spin-up case. The crystal-field and *sp*-hybridization split the Mn 3*d*-states into several bands. For the spin-up case two peaks on PDOS are resolved according to *e_g*-symmetry (centered at $E_{\text{VBM}} - 4.1$ eV) and *t_{2g}*-symmetry (centered at $E_{\text{VBM}} - 4.5$ eV). The 3*d*-states with *e_g*-symmetry are only slightly broadened by hybridization, while the *t_{2g}*-states are strongly hybridized with the Te 5*p*-states. The corresponding two peaks for the spin-down case are centered at $E_{\text{VBM}}+2.2$ eV and $E_{\text{VBM}}+2.8$ eV, respectively. We define two exchange splitting, separately for *e_g*- and *t_{2g}*-symmetry, as the separation between the corresponding spin-up and spin-down peaks: $\Delta e_g=6.3$ eV and $\Delta t_{2g}=7.3$ eV. Our results compare well with GW calculations ($\Delta e_g=6.2$ eV and $\Delta t_{2g}=6.7$ eV [34]) and are close to the experimental exchange splitting of the Mn 3*d*-levels of ~ 6.9 eV [40].

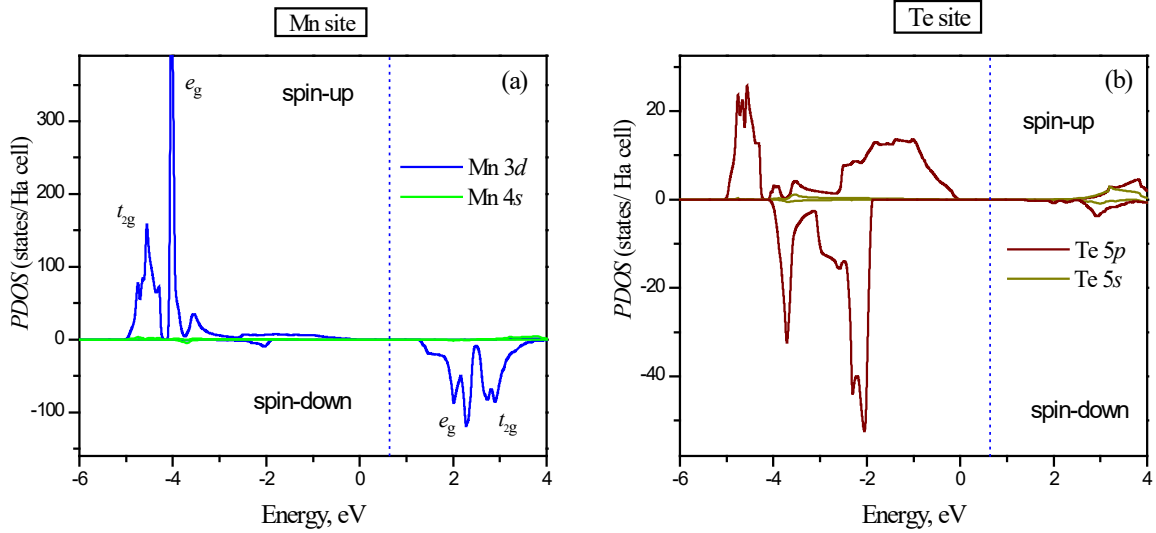


Fig. 3. Partial density of states for MnTe in the ferromagnetic phase for the spin-up and spin-down cases: (a) Mn site, and (b) Te site. The dotted line shows the position of the Fermi energy.

The calculations show that VBM for the spin-down structure is situated below the VBM for the spin-up structure, which gives negative and large spin-splitting $\Delta E_v = \Delta E_v^\downarrow - \Delta E_v^\uparrow = -1.91$ eV. The situation for the conduction band is opposite: $\Delta E_c = \Delta E_c^\downarrow - \Delta E_c^\uparrow = 0.41$ eV. The negative splitting of the VBM is a consequence of the strong Mn Hubbard-*U* repulsion and indicates that the effective potential for the minority spin is more attractive than that for the majority spin [1, 2].

The predicted band-edge spin-splitting ΔE_c and ΔE_v of the CBM and VBM at the G point can be used to estimate the *sp-d* exchange constants $N_0\alpha$ and $N_0\beta$. These parameters describe the exchange interactions between electron carriers of the valence and conduction bands and the Mn spin and are defined by the relations:

$$N_0\alpha = \Delta E_c / x\langle S \rangle, \quad N_0\beta = \Delta E_v / x\langle S \rangle. \quad (1)$$

Here x is the concentration of Mn ($x = 1$ in our case), and $\langle S \rangle$ is one-half of the total spin on the magnetic ion. Due to the hybridization, the local magnetic moment of the Mn is less than the free space value $5\mu_B$. In our calculation, the total magnetic moment within the Mn PAW sphere is $4.42 \mu_B$. The calculated values of the exchange constants and spin-splitting of the conduction and the valence bands for MnTe are given in Table 1. Our results obtained within GGA+ U^{SIC} method are close to the commonly accepted values of $N_0\alpha = 0.22$ eV and $N_0\beta = -0.88$ eV for the valence and conduction band, respectively [39].

4. STRUCTURAL, ELECTRONIC AND MAGNETIC PROPERTIES OF Cd_{1-x}Mn_xTe

4.1 Structural properties of Cd_{1-x}Mn_xTe

The Cd_{1-x}Mn_xTe alloy in ferromagnetic phase was modelled using 8-atom supercells for the compositions of $x = 0.25$, 0.75, and 16-atom supercell for the composition of $x = 0.5$. For these structures, the total energies for different volumes around the equilibrium volume cell were fitted to the Murnaghan's equation of state. The obtained equilibrium lattice constant and the bulk modulus of ferromagnetic Cd_{1-x}Mn_xTe alloy are given in Table 2. In going from CdTe to MnTe, when the Mn content increases, the values of Cd_{1-x}Mn_xTe lattice constant decrease. This is due to the smaller size of the Mn atom in comparison to the Cd atom. Fig. 4 show the variation of the calculated equilibrium lattice constant versus composition x for Cd_{1-x}Mn_xTe alloy. Our calculated lattice constants were found to vary almost linearly following the Vegard's law. The slight increase of the bulk modulus B by increasing the Mn content can be explained by the fact that the bond length becomes shorter when incorporating more Mn atoms and is an indication that the Cd_{1-x}Mn_xTe alloy becomes harder.

Table 2. Calculated lattice constant a (in Å) and bulk modulus B (in GPa) for Cd_{1-x}Mn_xTe alloy.

Composition (x)	0.25		0.5		0.75	
	a (Å)	B (GPa)	a (Å)	B (GPa)	a (Å)	B (GPa)
Present	6.488	43.57	6.44	44.48	6.396	45.56
[16]	6.354	47.1				
[15]			6.32	49.94		
[36]					6.421	37.12

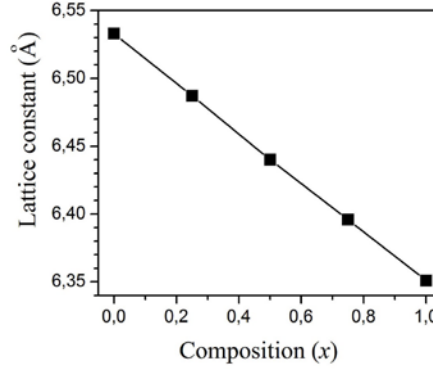


Fig. 4. Calculated lattice constant a for Cd_{1-x}Mn_xTe alloy as a function of Mn content.

4.2 Electronic and magnetic properties of Cd_{1-x}Mn_xTe

The electronic band structure calculations within the GGA+U^{SIC} method of Cd_{1-x}Mn_xTe alloy for compositions $x = 0.25$, 0.5, 0.75 show that both the top of the valence band and the bottom of the conduction band are located at the G point of the Brillouin zone, in agreement with the pure CdTe and MnTe band structures. That is, ferromagnetic Cd_{1-x}Mn_xTe has a direct band gap at the G point. Composition dependencies of the calculated band gap E_g for the spin-up and spin-down cases are presented in Figure 5. The calculated band gap values for Cd_{1-x}Mn_xTe are 2.29 eV ($x = 0.25$), 2.93 eV ($x = 0.5$), 3.54 eV ($x = 0.75$), 4.10 eV ($x = 1$) in the case of the spin-up structure, and 1.64 eV ($x = 0.25$), 1.67 eV ($x = 0.5$), 1.72 eV ($x = 0.75$), 1.79 eV ($x = 1$) in the case of the spin-down structure. Figure 5 shows that increasing Mn content leads to an increase of the band gap with a downward bowing for the spin-up case and upward bowing for the spin-down case. The calculated band gaps versus concentrations can be represented by the polynomial form:

$$E_g(x) = xE_{\text{MnTe}} + (1-x)E_{\text{CdTe}} + bx(1-x), \quad (2)$$

where E_{MnTe} and E_{CdTe} correspond to the band gaps of MnTe and CdTe, respectively, and b is a bowing parameter. The equation (2), fitted with the calculated band gap data, yields to the band gap bowing parameter $b = -0.07$ eV, which is relatively small for the spin-up case, while that for spin-down case is rather large $b = 0.31$ eV.

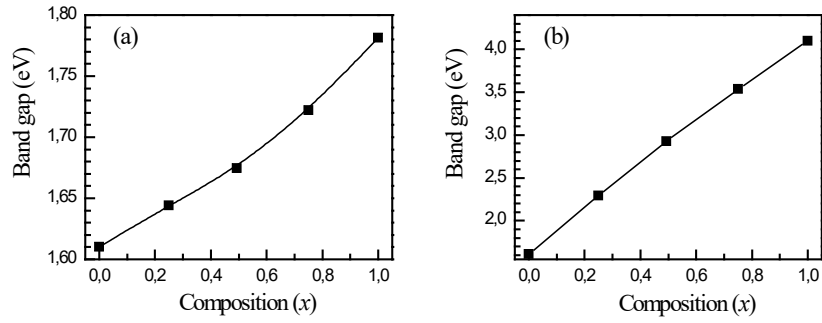


Fig. 5. Calculated band gap of $\text{Cd}_{1-x}\text{Mn}_x\text{Te}$ alloy as a function of the Mn content for the spin-up (a) and spin-down (b) cases.

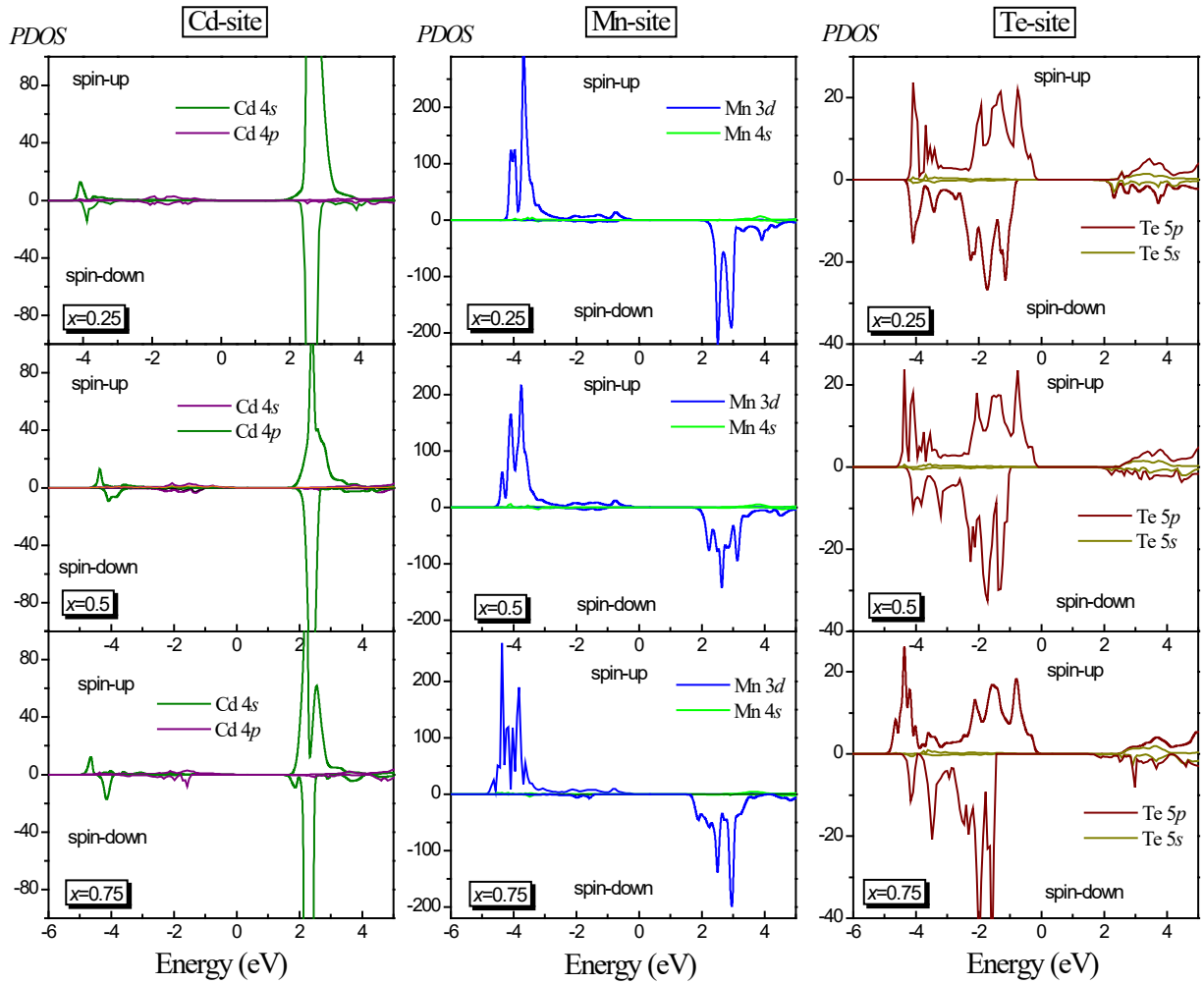


Fig. 6. Partial density of states of $\text{Cd}_{1-x}\text{Mn}_x\text{Te}$ alloy for compositions $x = 0.25, 0.5, 0.75$.

For the qualitative analysis of the atomic and orbital origins of different $\text{Cd}_{1-x}\text{Mn}_x\text{Te}$ band states, we evaluated the spin-dependent PDOS. Fig. 6 displays the PDOS of ferromagnetic $\text{Cd}_{1-x}\text{Mn}_x\text{Te}$ alloy for compositions of $x = 0.25, 0.5, 0.75$. The results obtained for the Cd, Mn and Te are situated within corresponding PAW sphere. For the sake of comparison, the energy zero of the band structure for all alloys is placed at the VBM of MnTe ($x = 1$) for the spin-up case. One can see that the valence band of the alloys for the spin-up case is formed predominantly from the unoccupied Cd 4s-states. The position of the corresponding peak in the density of states remains unchanged and somewhat broadens with a decrease of the Mn content. The bottom of the conduction band for the spin-down structure is dominated by the unoccupied Mn 3d-states, but there is also a contribution of the unoccupied Cd 4s-states. The position of the peaks corresponding to the Mn and Cd states does not change with an increase of the Mn content, but a small broadening of the Mn peak can be observed. The occupied states of the valence band for the spin-up structure are formed predominantly by the Mn 3d-orbitals and Te 5p-orbitals. Strong *sp-d* hybridization shifts the Mn band to the lower energies with increasing Mn content. The position of the peak shifts from $E_{\text{VBM}} - 4.1$ eV (for $x = 0.25$) to $E_{\text{VBM}} - 4.4$ eV (for $x = 0.75$). For the spin-down structure, the occupied states of the valence band are formed primarily from the Te 5p-orbitals. The band, corresponding to the strongly delocalized Te 5p-states, shifts with the Mn content to the lower energies similarly to the Mn band.

The calculated values of the magnetic moment, spin-splitting of the conduction and valence bands and the exchange constants $N_0\alpha, N_0\beta$ for $\text{Cd}_{1-x}\text{Mn}_x\text{Te}$ alloy for compositions $x = 0.25, 0.5, 0.75$ are listed in Table 3 along with the results of other studies. Our results show that total magnetic moment of the Mn in $\text{Cd}_{1-x}\text{Mn}_x\text{Te}$ alloy is slightly reduced from $4.42 \mu_B$ in MnTe to $4.40 \mu_B$ and is independent on the Mn content. The *sp-d* exchange splitting varies almost linearly with increasing x providing independence of the exchange constants on the alloy composition.

Table 3. Calculated magnetic moment μ (in Bohr magneton μ_B), conduction ΔE_c and valence ΔE_v (in eV) band-edge spin-splitting, and exchange constants $N_0\alpha, N_0\beta$ (in eV) of ferromagnetic $\text{Cd}_{1-x}\text{Mn}_x\text{Te}$ alloy.

Composition (x)	μ (μ_B)	$\Delta E_c, \Delta E_v$ (eV)	$N_0\alpha, N_0\beta$ (eV)	Reference
0.25	4.41	-0.49, 0.16	-0.89, 0.29	Present
	4.21	-0.80, 0.242	-1.28, 0.387	PBE-GGA [16]
0.5	4.40	-0.94, 0.33	-0.86, 0.30	Present
	4.326	-1.57, 0.46	-0.63, 0.19	PBE-GGA [15]
			-1.30, 0.54	PW-GGA [37]
0.75	4.40	-1.42, 0.39	-0.86, 0.24	Present
	4.087	-1.83, 0.36	-1.19, 0.23	PBE-GGA [36]

5. SUMMARY

In the present work, we apply the GGA+U^{SIC} method to calculate the structural, electronic and magnetic properties of pure CdTe, ferromagnetic MnTe and $\text{Cd}_{1-x}\text{Mn}_x\text{Te}$ alloy. Considering the explicitly on-site Hubbard U corrections together with self-interaction correction potential leads to a better description of the structural properties and electronic band structures of CdTe and ferromagnetic MnTe in the zinc-blende phase. The calculated values of lattice constant and band gap of CdTe and MnTe within the GGA+U^{SIC} method are close to the experimental ones, especially in comparison with the calculations within the conventional GGA approach. The structural, electronic and magnetic properties of $\text{Cd}_{1-x}\text{Mn}_x\text{Te}$ alloy were studied for selected compositions of $x = 0.25, 0.5, 0.75$ using a supercell method. We identified the compositional dependence of the lattice constant, band structure, and the total and partial densities of states of the alloy. The calculated lattice constants were found to vary almost linearly on x following Vegard's law. Increasing the Mn content leads to an increase of the energy band gap of the alloy with a small downward bowing for the spin-up case and upward bowing for the spin-down case. The study of $\text{Cd}_{1-x}\text{Mn}_x\text{Te}$ partial density of states revealed that the occupied states of the valence band for the spin-up structure are formed predominantly by the Mn 3d-orbitals and Te 5p-orbitals. Strong *sp*-hybridization shifts the Mn band to the lower energies with increasing Mn content. For the spin-down

structure the occupied states of the valence band are formed primarily from the Te $5p$ -orbitals, and the corresponding band shifts with an increase of the Mn content to lower energies. The calculated values of the magnetic moment and predicted spin-splitting of the conduction and the valence bands and exchange constants $N_0\alpha$, $N_0\beta$ for $\text{Cd}_{1-x}\text{Mn}_x\text{Te}$ alloy show that the sp - d exchange splitting varies almost linearly with x , providing that the exchange constants are independent of the Mn content.

REFERENCES

- [1] Kossut, J. and Gaj J.A., [Introduction to the Physics of Diluted Magnetic Semiconductors], Springer-Verlag, Berlin & Heidelberg, 1–36 (2010).
- [2] Dietl, T., “A ten-year perspective on dilute magnetic semiconductors and oxides”, *Nat. Mater.* 9, 965–974 (2010).
- [3] Triboulet, R. and Siffert, P., [CdTe and Related Compounds; Physics, Defects, Hetero- and Nano-structures, Crystal Growth, Surfaces and Applications], Elsevier, Amsterdam, 1–144 (2010).
- [4] Sato, H., Onodera, K. and Ohba, H., “Characterization of $\text{Cd}_{1-x}\text{Mn}_x\text{Te}$ crystals grown by the Bridgman method and the zone melt method”, *J. Cryst. Growth* 214/215, 885–888 (2000).
- [5] Mycielski, A., Kowalczyk, L., Galazka, R.R., Sobolewski, R., Wang, D., Burger, A., Sowinska, M., Groza, M., Siffert, P., Szadkowski, A., Witkowska, B. and Kaliszek, W., “Applications of II–VI semimagnetic Semiconductors”, *J. Alloys Compd.* 423, 163–168 (2006).
- [6] Hwang, Y., Chung, S. and Um, Y., “Giant Faraday rotation in $\text{Cd}_{1-x}\text{Mn}_x\text{Te}$ ($0 < x < 0.82$) crystals”, *Phys. Stat. Sol. C*, 4, 4453–4456 (2007).
- [7] Cui, Y., Bolotnikov, A., Hossain, A., Camarda, G., Mycielski, A., Yang, G., Kochanowska, D., Witkowska-Baran, M. and James, R.B., “CdMnTe in X-ray and gamma-ray detection: potential applications”, *Proc. SPIE*, Vol. 7079, (2008).
- [8] Kim, K.H., Tappero, R., Bolotnikov, A.E., Hossain, A., Yang, G., James, R.B. and Fochuk, P., “Long-term stability of ammonium-sulfide- and ammonium-fluoride-passivated CdMnTe detectors”, *J. of the Korean Phys. Soc.* 66 (10), 1532–1536 (2015).
- [9] Nikonyuk, E.S., Zakharuk, Z.I., Kuchma, M.I., Rarenko, A.I., Shlyakhovyi, V.L. and Yuriychuk I.M., “Relaxation processes in conductivity of $\text{Cd}_{1-x}\text{Mn}_x\text{Te}$ crystals ($0.02 < x < 0.55$)”, *Semiconductors* 42 (9), 1012–1015 (2008).
- [10] Nykoniuk, Ye., Solodin, S., Zakharuk, Z., Dremlyuzhenko, S., Rudyk, B. and Fochuk, P., “Compensated donors in semi-insulating $\text{Cd}_{1-x}\text{Mn}_x\text{Te}:\text{In}$ crystals”, *J. Cryst. Growth* 500, 117–121 (2018).
- [11] Hass, K.C., Larson, B.E., Ehrenreich, H. and Carlsson, A.E., “Magnetic interactions in diluted magnetic semiconductors”, *J. Magn. Magn. Mater.* 54, 1283–1284 (1986).
- [12] Wei, S.H. and Zunger, A., “Total-energy and band-structure calculations for the semimagnetic $\text{Cd}_{1-x}\text{Mn}_x\text{Te}$ semiconductor alloy and its binary constituents”, *Phys. Rev. B* 35, 2340–2365 (1987).
- [13] Wei, S.-H., Gong, X.G., Dalpian, G.M. and Wei, S.H., “First-principles study of Mn-induced local magnetic moments in host semiconductors”, *Phys. Rev. B* 71, 144409–144414 (2005).
- [14] Sharma, S., Devi, N., Verma, U.P. and RajaRam, P., “Ab-initio investigations of structural, electronic, magnetic and optical properties of ferromagnetic $\text{Cd}_{1-x}\text{Mn}_x\text{Te}$ ”, *Phys. B* 406, 4547–4553 (2011).
- [15] Touat, S.A., F. Litimein, S.A., Tadjer, A. and Bouhafs, B., “The spin effect in zinc-blende $\text{Cd}_{0.5}\text{Mn}_{0.5}\text{Te}$ and $\text{Cd}_{0.5}\text{Zn}_{0.5}\text{Te}$ diluted magnetic semiconductors: FP-LAPW study”, *Physica B* 405, 625–631 (2010).
- [16] Merad, A.E., Kanoun, M.B. and Goumri-Said, S., “Ab initio study of electronic structures and magnetism in ZnMnTe and CdMnTe diluted magnetic semiconductors”, *J. Magn. Magn. Mater.* 302, 536–542 (2006).
- [17] Raiss, A. Ait, Sbai, Y., Bahmad L. and Benyoussef A., “Magnetic and magneto-optical properties of doped and co-doped CdTe with (Mn, Fe): Ab-initio study”, *J. Magn. Magn. Mater.* 385, 295–301 (2015).
- [18] Gueddim, A., Madjet, M.E., Zerroug, S. and Bouarissa N., “First-principles investigations of electronic properties and optical spectra of $\text{Cd}_{1-x}\text{Mn}_x\text{Te}$ dilute magnetic semiconductors”, *Opt. Quant. Electron.* 48, 551–563 (2016).
- [19] Radisavljevic, I., Novakovic, N., Romcevic, N., Mitric, M., Kuzmanovic, B., Bojanic, S. and Ivanovic N., “Electronic aspects of formation and properties of local structures around Mn in $\text{Cd}_{1-x}\text{Mn}_x\text{Te}_{1-y}\text{Se}_y$ ”, *Mater. Chem. Phys.* 167, 236–245 (2015).
- [20] Anisimov, V.I., Zaanen, J. and Andersen, O.K., “Band theory and Mott insulators: Hubbard U instead of Stoner I ”, *Phys. Rev. B* 44, 943–954 (1991).

- [21] Stephens, P.J., Devlin F.J., Chabalowski C.F. and Frisch M.J., “Ab Initio Calculation of Vibrational Absorption and Circular Dichroism Spectra Using Density Functional Force Fields”, *J. Phys. Chem. Lett.* 98 (45), 11623–11627 (1994).
- [22] Heyd, J., Scuseria, G.E. and Ernzerhof, M., “Hybrid functionals based on a screened Coulomb potential”, *J. Chem. Phys.* 118, 8207–8215 (2003).
- [23] Rinke, P., Qteish, A., Neugebauer, J., Freysoldt, C. and Scheffler M., “Combining GW calculations with exact-exchange density-functional theory: an analysis of valence-band photoemission for compound semiconductors”, *New J. Phys.* 7, 126 (2005).
- [24] Perdew, J.P. and Zunger, A., “Self-interaction correction to density-functional approximations for many-electron systems”, *Phys. Rev. B* 23, 5048-5079 (1981).
- [25] Persson, C. and Mirbt, S., “Improved electronic structure and optical properties of *sp*-hybridized semiconductors using LDA+U^{SIC}”, *Brazil. J. Phys.* 36, 286–290 (2006).
- [26] Menéndez-Proupin, E., Amézaga, A. and Cruz Hernández, N., “Electronic structure of CdTe using GGA-U^{SIC}”, *Physica B* 452, 119–123 (2014).
- [27] Gonze, X., Jollet, F., Abreu Araujo, F., Adams, D., Amadon, B., Applencourt, T., Audouze, C., Beuken, J.-M., Bieder, J., Bokhanchuk, A., Bousquet, E., Bruneval, F., Caliste, D., Côté, M., Dahm, F., Da Pieve, F., Delaveau, M., Di Gennaro, M., Dorado, B., Espejo, C., Geneste, G., Genovese, L., Gerossier, A., Giantomassi, M., Gillet, Y., Hamann, D.R., He, L., Jomard, G., Laflamme Janssen, J., Le Roux, S., Levitt, A., Lherbier, A., Liu, F., Lukacevic, I., Martin, A., Martins, C., Oliveira, M.J.T., Poncé, S., Pouillon, Y., Rangel, T., Rignanese, G.-M., Romero, A.H., Rousseau, B., Rubel, O., Shukri, A.A., Stankovski, M., Torrent, M., Van Setten, M.J., Van Troeye, B., Verstraete, M.J., Waroquier, D., Wiktor, J., Xue, B., Zhou, A. and Zwanziger, J.W., “Recent developments in the ABINIT software package”, *Computer Phys. Comm.* 205, 106–131 (2016).
- [28] Perdew, J.P., Burke, K. and Ernzerhof, M., “Generalized Gradient Approximation Made Simple”, *Phys. Rev. Lett.* 77, 3865–3868 (1996).
- [29] Kresse, G. and Joubert, D., “From ultrasoft pseudopotentials to the projector augmented-wave method”, *Phys. Rev. B* 59, 1758–1775 (1999).
- [30] Monkhorst, H.J. and Pack, J.D., “Special points for Brillouin-zone integrations”, *Phys. Rev. B* 13, 5188–5192 (1976).
- [31] Zunger, A, Wei, S.H., Feireira, L.G. and Bernard J.E., “Special quasirandom structures”, *Phys. Rev. Lett.* 65, 353–356 (1990).
- [32] Madelung, O., Schultz, M. and Weiss, H., [Landolt-Bornstein: Numerical Data and Functional Relationships in Science and Technology], Berlin, Springer-Verlag 17b (1982).
- [33] Heyd, J., Peralta, J.E., Scuseria, G.E. and Martin, R.L., “Energy band gaps and lattice parameters evaluated with the Heyd-Scuseria-Ernzerhof screened hybrid functional”, *J. Chem. Phys.* 123, 174101 (2005).
- [34] Fleszar, A., Potthoff, M. and Hanke, W., “Electronic structure of zinc-blende MnTe within the GW approximation”, *Phys. Stat. Sol. C* 4 (9), 3270–3279 (2007).
- [35] Krause, M. and Bechstedt, F., “Structural and magnetic properties of MnTe phases from ab initio calculations”, *J. Supercond. Nov. Magn.* 26, 1963–1972 (2013).
- [36] Verma, U.P., Sharma, S., Devi, N., Bisht, P.S. and Rajaram P., “Spin polarized structural, electronic and magnetic properties of diluted magnetic semiconductors (Cd,Mn)Te in zinc blende phase”, *J. Magn. Magn. Mater.* 323, 394–399 (2011).
- [37] Wei, S. H., Gong, X.G., Dalpian, G.M. and Wei, Su.H., “First-principles study of Mn-induced local magnetic moments in host semiconductors”, *Phys. Rev. B* 71 144409–144414 (2005).
- [38] Janik, E., Dynowska, E., Bak-Misiuk, J., Leszczynski, M., Szuszkiewicz, W., Wojtowicz, T., Karczewski, G., Zakrzewski, A.K. and Kossut, J., “Structural properties of cubic MnTe layers grown by MBE”, *Thin Solid Films* 267, 74–78 (1995).
- [39] Gaj, J.A., Planel, R. and Fishman, G., “Relation of magneto-optical properties of free excitons to spin alignment of Mn²⁺ ions in Cd_{1-x}Mn_xTe”, *Sol. State Commun.* 29, 435–438 (1979).
- [40] Mimura, K., Sato, H., Senba, S., Namatame, H. and Taniguchi, M., “Ultraviolet inverse-photoemission and photoemission spectroscopies of zincblende MnTe”, *Physica B* 237–238, 392–393 (1997).